JOURNAL OF AIRCRAFT
Vol. 44, No. 3, May–June 2007

CFD-Based Models of Aerodynamic Gust Response

Daniella E. Raveh*
Technion—Israel Institute of Technology, 32000 Haifa, Israel

DOI: 10.2514/1.25498

The paper presents a novel approach to modeling unsteady aerodynamic forces in response to traveling gust excitation. Time-domain convolution, autoregressive moving average, and state-space models are presented that are identified based on CFD input–output data. These models are compact and computationally efficient and reproduce the CFD response highly accurately in the subsonic flow regime. The proposed models can be straightforwardly integrated into the time-domain formulation of the aeroelastic equation of motion in response to gust excitation. They can be used for both discrete and continuous gust responses, as presented in the paper.

Nomenclature

$a_1, \cdots, a_{n_a}, b_0, b_1, \cdots, b_{n_b}$	=	autoregressive moving average model coefficients
c	=	chord length
F	=	aerodynamic response
$\hat{F}$	=	aerodynamic response predicted by autoregressive moving average model
$\tilde{F}$	=	autoregressive moving average model prediction error
f	=	gust velocity distribution profile in the flight direction
f_s, f_{Nyq}	=	sampling and Nyquist frequencies
$\boldsymbol{GF}_A$	=	generalized aerodynamic forces, normalized by q
$\boldsymbol{GF}_G$	=	gust-generalized aerodynamic forces, normalized by q
GK	=	generalized stiffness
GM	=	generalized mass
k	=	reduced frequency
M	=	Mach number
N	=	length of the training data
n	=	discrete-time step
n_a, n_b	=	autoregressive moving average model orders
P_{xx}	=	cross/power-spectral density
q	=	dynamic pressure
t	=	time
V	=	flight speed
$w_g, \bar{w}_g$	=	gust velocity, gust velocity amplitude
x	=	chordwise coordinate
x_A, x_S, x_{SA}, x_G	=	aerodynamic, structural, aeroelastic, and gust states in state-space models
x_{SAG}	=	states of the aeroelastic system with gust augmented
ξ	=	generalized displacement
$[\phi]$	=	modes matrix
$\psi(t)$	=	aerodynamic forces in response to sharp-edged gust excitation
ω	=	angular velocity

Presented as Paper 2022 at the 47th Structures, Structural Dynamics and Materials Conference, Newport, RI, 1–4 May 2006; received 30 May 2006; revision received 29 August 2006; accepted for publication 31 August 2006.

*Senior Lecturer, Faculty of Aerospace Engineering. Member AIAA.

I. Introduction

GUST-RESPONSE analysis plays a major role in aircraft structural design, as gust loads typically control the wing design of large aircraft. The Federal Aviation Regulations [1] (FARs) require that the aircraft structure can withstand discrete gusts of certain profile, intensity, and gradient. Aeroelastic effects, which have significant influence on gust loads, must be accounted for in the dynamic gust analysis. Modern methods for dynamic gust analysis typically rely on panel-method aerodynamics [2]. Frequency-domain aerodynamics are used in conjunction with the frequency-domain formulation of the aeroelastic equation of motion in generalized coordinates. The gust velocity input is expressed as a combination of harmonic excitations of various reduced frequencies, and the gust-generalized aerodynamic forces are computed using the generalized aerodynamic influence coefficient matrices (AICs) at these reduced frequencies. For time-response simulation, or for aeroservoelastic analysis, time-domain state-space (SS) models are extracted by rational function approximation [3,4] or other reduced-order modeling techniques [5]. However, this extraction is not straightforward [3,5]. Section loads (shear forces and bending moments at span sections) that are required for structural analysis and design are computed by summation of the aerodynamic and inertial loads outboard of the section (summation-of-forces approach) or from the elastic deformations and stiffness matrix (mode-displacement approach).

Tang et al. [6] presented a method for proper orthogonal decomposition and SS modeling of the unsteady aerodynamic forces due to gust excitation. SS models were identified based on the aerodynamic response of a delta wing to sharp-edged and swept-gust excitations, which were computed by a vortex lattice code. The SS models were shown to accurately reproduce the system's response and capture the eigenmodes of the original vortex lattice system.

The current study aims at exploiting the now-available CFD tools for dynamic gust-response analysis. CFD codes are typically thought of as tools for nonlinear flows. In this study, however, the exploitation of CFD tools for both nonlinear and linear flows, at all flow regimes, is suggested. This is achieved by using a combination of full CFD simulations and reduced-order models (ROMs) that together offer models of various fidelity for gust-response analysis. In a recent study by the author [7], the elastic zonal Navier–Stokes simulation [8] (EZNSS) CFD code was enhanced to simulate the time history of the aerodynamic response of an airfoil to arbitrary gust inputs. Validation was achieved by comparison of the simulated lift responses to a step angle of attack (AOA) and a sharp-edged gust to the closed-form Wagner and Küssner functions, respectively, at subsonic and transonic flow regimes. Time-domain ROMs of the autoregressive moving average (ARMA) type were identified from a set of CFD input–output data. Responses to gust inputs of various shape, intensity, and gradient length were estimated using the ROMs and compared with responses from direct CFD simulations. For the airfoils studied in [7], the ROMs proved to be a powerful tool for accurately predicting gust responses at computational cost that is

significantly smaller than that of full CFD simulation. The studies of [6,7] laid the basic validation and proof of concept for CFD-based gust-response simulation and the use of ROMs for gust analysis. In the current study, we wish to explore dynamic gust simulation and reduced-order modeling of three-dimensional wings.

The current study aims at the identification of ROMs for the response of a rigid three-dimensional wing to a traveling gust excitation and its coupling with the aeroelastic equation of motion. Four ROMs are developed: a convolution model that is based on CFD-computed sharp-edged gust response, two parametric ARMA and SS models, and a frequency-response model. Models of the lift coefficient, root-bending moment (RBM), and gust-generalized aerodynamic forces are developed and used to compute responses to discrete and continuous gust excitations. Validation is achieved through comparison of the responses from these models to those computed directly in CFD simulations.

II. Methodology

The aeroelastic equation of motion in response to atmospheric gust excitation in generalized coordinates, neglecting damping, is stated as

$$GM\ddot{\xi} + GK\xi - q\boldsymbol{GF}_A(t) = q\boldsymbol{GF}_G(t) \tag{1}$$

The generalized aerodynamic forces (GAFs) are dependent on the structural deformations, their time histories, and on the time histories of the generalized aerodynamic forces themselves. The gust-generalized aerodynamic forces (GGAFs) are due to discrete traveling gust excitation. They are dependent on the velocity profile of the gust input and on the histories of the gust forces. The gust is an external excitation and, therefore, the gust forces are independent of the structural deformations. Reference [9] presented CFD-based ROMs of the GAFs. The current study is focused on the development of CFD-based ROMs for the GGAFs. Various models are developed that fit different formulations of Eq. (1). These include a time-domain convolution model, time-domain parametric ARMA and SS models, and a frequency-domain model, described in the following subsections.

A. Gust Convolution Model

We consider a discrete gust with an arbitrary velocity distribution profile in the flight direction and a uniform velocity distribution in the spanwise direction, shown in Fig. 1. The gust travels over a wing at the constant flight speed, starting from the wing root leading edge at time zero. This gust induces at t, at location x on the wing, a vertical velocity of

$$w_g(t)\begin{cases} \bar{w}_g f\left(t - \frac{x}{V}\right) & t > \frac{x}{V} \\ 0 & t < \frac{x}{V} \end{cases} \tag{2}$$

The resulting GGAF can be evaluated by convolution, according to

$$\{\boldsymbol{GF}_G(t)\} = \frac{1}{q}\int_0^t \dot{w}_g(\tau) G\psi(t-\tau)\,\mathrm{d}\tau \tag{3}$$

where $\dot{w}_g$ is the time derivative of the gust input velocity at the leading edge,

$$G\psi(t) = [\phi]^T\{\psi(t)\} \tag{4}$$

is the time-dependent modal force response due to a sharp-edged gust excitation; $\psi(t)$ holds the time-dependent aerodynamic forces, computed at the CFD grid points, in response to a sharp-edged gust excitation of unit amplitude; and for $[\phi]$, each column represents an elastic mode shape. The mode shapes, which are typically computed by finite elements at the finite element model nodes, are mapped to the geometrical points at which the gust forces are evaluated, in order to perform the matrix multiplication of Eq. (4). When $\{\phi\}$ is a unit-displacement heave mode, the generalized gust force of Eq. (4) is the time-dependent total lift due to the sharp-edged gust. Similarly, the RBM due to the sharp-edged gust can be computed by using a mode that holds the moment arms from each CFD grid to the wing root (a "load mode").

A sharp-edged gust profile, encountered at the wing root leading edge at time zero, induces at t, at x on the wing, a vertical velocity of

$$w_g(t) = \begin{cases} \bar{w}_g & t > \frac{x}{V} \\ 0 & t < \frac{x}{V} \end{cases} \tag{5}$$

A method of introducing gust excitation to CFD computations was recently proposed by Parameswaran and Baeder [10] and practiced by Singh and Baeder [11,12] and by Zaide and Raveh [7]. The method, named the field velocity method, introduces vertical gust velocities to the CFD computation by assigning the gust velocities to the CFD grid time metrics, without actually moving the grid. The sharp-edged gust excitation is introduced to the flow analysis by prescribing the gust vertical velocity $\bar{w}_g$ to all grid points with a flow-direction coordinate x of $x \le tV$.

The GGAF computed by Eq. (3) can be introduced into the aeroelastic equation (1) to form the aeroelastic gust-response equation:

$$GM\ddot{\xi} + GK\xi - q\boldsymbol{GF}_A(t) = \frac{1}{q}\int_0^t \dot{w}_g(\tau) G\psi(t-\tau)\,\mathrm{d}\tau \tag{6}$$

Equation (6) can be solved for ξ using numerical integration schemes. Because the excitation force on the right-hand side is independent of the displacements, it can be computed in advance and independently of the ROM technique used for the estimation of the aerodynamic forces due to elastic deformations on the left-hand side. For example, the $\boldsymbol{GF}_A$ term can be computed using convolution, based on Wagner's closed-form step-AOA response.

B. ARMA and State-Space Gust Models

The gust ARMA model relates the gust response to the gust velocities at the current and previous time steps and to previous time-step values of the response. For a single response, it assumes the following model structure:

$$\begin{aligned} F(n) = &-a_1F(n-1) - a_2F(n-2) - \cdots - a_{n_a}F(n-n_a) \\ &+ b_0w_g(n) + b_1w_g(n-1) + \cdots + b_{n_b}w_g(n-n_b) \end{aligned} \tag{7}$$

where w_g is the value at the leading edge at n, and F is a response of the rigid wing. The responses F in this study will be the lift coefficient, the RBM, and the GGAF associated with the wing's elastic modes. In general, ARMA models can be fitted to represent various responses, such as the pressure at a certain wing location or any section load. The model orders n_a and n_b are determined by the user, and $a_1, \cdots, a_{n_a}$, $b_0, b_1, \cdots, b_{n_b}$ are the model parameters to be estimated.

From Eq. (7), the predicted output $\hat{F}$ can be posed as

$$\hat{F} = \boldsymbol{H}^T(n)\hat{\theta} \tag{8}$$

where $\boldsymbol{H}$ is the regression vector

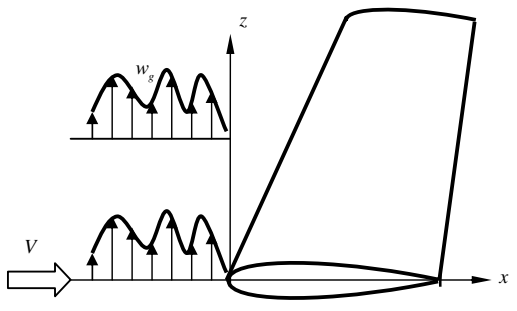

Fig. 1 Traveling gust excitation.

$$\boldsymbol{H} = [-F(n-1) \quad -F(n-2) \quad \cdots \quad -F(n-n_a) \quad w_g(n) \quad w_g(n-1) \quad \cdots \quad w_g(n-n_b)]^T \tag{9}$$

and

$$\hat{\theta}^T = [a_1 \quad a_2 \quad \cdots \quad a_{n_a} \quad b_0 \quad b_1 \quad \cdots \quad b_{n_b}] \tag{10}$$

The prediction error $\tilde{F}$ is defined as

$$\tilde{F} = F - \hat{F} = F - \boldsymbol{H}^T(n)\hat{\theta} \tag{11}$$

where F is the measured output. The parameters that minimize the prediction error of Eq. (11) in a least-squares sense are given by (see [13], Chapter 7.3, pages 203–211)

$$\hat{\theta} = \arg \min\left\{\frac{1}{N}\sum_{n=1}^{N}\tilde{F}^2\right\} = \boldsymbol{H}^T\boldsymbol{H})^{-1}\boldsymbol{H}^T F \tag{12}$$

where N is used for parameter identification, that is, the number of iterations in the CFD analysis that generated the training data.

Zaide and Raveh [7] identified an ARMA gust model of the lift coefficient on an airfoil. A model size of $n_a = 2$ and $n_b = 1$ was chosen, because the approximation of the closed-form Küssner function for the flat-plate lift gust response can be expressed as a 2,1 ARMA model. In the current study, the ARMA models of the 3-D wing are of the order of tens (presented in the Numerical Application section). Because the identification of model parameters from Eq. (12) is quick, several model orders can be tested to arrive at the best model order.

To introduce the GGAF into the aeroelastic equation of motion in SS formulation, the gust ARMA model can be posed in SS form, as

$$\begin{aligned} x_G(n+1) &= A_G x_G(n) + B_G w_g(n) \\ F_G(n) &= C_G x_G(n) + D_G w_g(n) \end{aligned} \tag{13}$$

where F_G represents the GGAF times the dynamic pressure. Equation (13) formulates the gust loads due to gust excitation, independent of the elastic motion.

C. State-Space Formulation of the Aeroelastic System

The aeroelastic equation of motion (1), excited by gust loads, can be presented as the block diagram of Fig. 2. The dashed box represents the aeroelastic system, with the aeroelastic feedback of aerodynamic forces due to elastic motion. From the left side comes the external excitation; in the current study, it is the load due to traveling gust. The system can be formulated in SS form as

$$\begin{aligned} \dot{x}_S(t) &= \bar{A}_S x_S(t) + \bar{B}_S F_A(t) + \bar{B}_{SG} F_G(t) \\ \xi(t) &= \bar{C}_S x_S(t) + \bar{D}_S F_A(t) + \bar{D}_{SG} F_G(t) \end{aligned} \tag{14}$$

where

$$x_S(t) = \begin{Bmatrix} \xi \\ \dot{\xi} \end{Bmatrix} \tag{15}$$

$$\bar{A}_S = \begin{bmatrix} 0 & I \\ -GM^{-1}GK & 0 \end{bmatrix} \qquad \bar{B}_S = \begin{bmatrix} 0 \\ GM^{-1} \end{bmatrix} \qquad \bar{B}_{SG} = \begin{bmatrix} 0 \\ GM^{-1} \end{bmatrix} \tag{16}$$

$$\bar{C}_S = [I \quad 0] \qquad \bar{D}_S = [0] \qquad \bar{D}_{SG} = [0] \tag{17}$$

and where F_A and F_G are the GAF and GGAF of Eq. (1) respectively, multiplied by the dynamic pressure. In discrete-time SS form, Eq. (14) reads [14]

$$\begin{aligned} x_S(n+1) &= A_S x_S(n) + B_S F_A(n) + B_{SG} F_G(n) \\ \xi(n) &= C_S x_S(n) \end{aligned} \tag{18}$$

where

$$A_S = e^{\bar{A}_S T} \qquad B_S = \int_0^T e^{\bar{A}_S \tau}\, \mathrm{d}\tau \bar{B}_S \qquad B_{SG} = \int_0^T e^{\bar{A}_S \tau}\, \mathrm{d}\tau \bar{B}_{SG} \qquad C_S = \bar{C}_S \tag{19}$$

Reference [9] presented a method by which a SS model of the GAF can be identified from CFD data and the aeroelastic system excited by initial conditions (the dashed box in Fig. 2) can be formulated and analyzed in SS. Following [9], the GAF SS model can be posed as

$$x_A(n+1) = A_A x_A(n) + B_A \xi(n) \qquad F_A(n) = C_A x_A(n) + D_A \xi(n) \tag{20}$$

This is augmented to the structure's equation (18) to yield the coupled aeroelastic system (the dashed box in Fig. 2):

$$x_{SA}(n+1) = A_{SA} x_{SA}(n) + B_{SA} F_G(n) \qquad \xi(n) = C_{SA} x_{SA}(n) \tag{21}$$

where the states of the aeroelastic system are

$$x_{SA} = \begin{Bmatrix} x_S \\ x_A \end{Bmatrix} \tag{22}$$

and

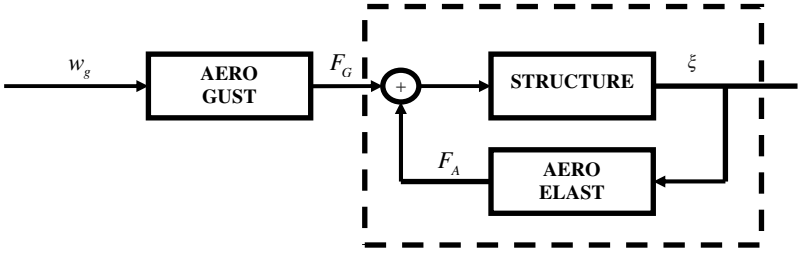

Fig. 2 Block diagram of the aeroelastic system with gust excitation.

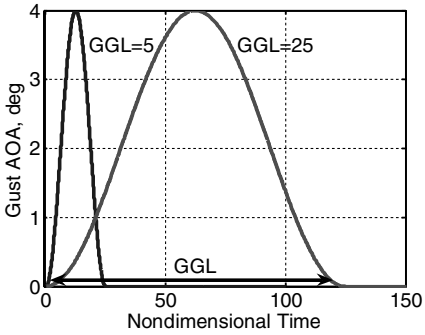

Fig. 3 One-minus-cosine gust excitations; Mach 0.2.

$$A_{SA} = \begin{bmatrix} A_S + B_S D_A C_S & B_S C_A \\ B_A C_S & A_A \end{bmatrix} \qquad B_{SA} = \begin{bmatrix} B_{SG} \\ 0 \end{bmatrix} \qquad C_{SA} = [\, C_S \quad 0 \,] \tag{23}$$

The gust aerodynamic force system, Eq. (13), is augmented to Eq. (21) to yield the aeroelastic equation in response to gust excitation:

$$x_{SAG}(n+1) = \begin{Bmatrix} x_{SA}(n+1) \\ x_G(n+1) \end{Bmatrix} = \begin{bmatrix} A_{SA} & B_{SA} C_G \\ 0 & A_G \end{bmatrix} \begin{Bmatrix} x_{SA}(n) \\ x_G(n) \end{Bmatrix} + \begin{bmatrix} B_{SA} D_G \\ B_G \end{bmatrix} w_g(n)$$

$$\xi(n) = \begin{bmatrix} C_{SA} & D_{SG} C_G \end{bmatrix} \begin{Bmatrix} x_{SA}(n) \\ x_G(n) \end{Bmatrix} + \begin{bmatrix} D_{SG} & D_G \end{bmatrix} w_g(n) \tag{24}$$

D. System Identification Signal

The system identification process is similar to that described in [9] for the identification of the GAF due to elastic deformations, except that in the current study, the excitation is that of a traveling gust (vertical velocity input), rather than of elastic modal motions. The CFD code is run to compute the time histories of the lift coefficient, RBM, and four-mode GGAF responses of the rigid wing to the traveling excitation signal. These responses serve as the training data. When the training data are available, ARMA/SS model orders are determined by the user, and the model coefficients are identified following Eq. (12).

The training data are the CFD response to an input signal that is a random time series with Gaussian distribution, filtered to excite only the frequency spectrum of interest. This signal will be referred to as filtered white Gaussian noise (FWGN). The input signal is normalized to unit maximum amplitude and multiplied by the desired gust input AOA. The amplitude of the excitation signal should be small enough to avoid nonlinear response due to nonlinear phenomena, such as flow separation. On the other hand, the gust amplitude should not be too small, such that the response will not be in the order of magnitude of the computational errors. In the test cases of the current study, the maximum gust velocity amplitudes correspond to 2-, 4-, and 5-deg AOA. In the low subsonic flows, these low AOAs result in attached, linear flow. At transonic Mach numbers, a shock wave develops. However, because the flow analysis is inviscid (Euler), there is no flow separation, and the response is linear, or close to linear, with respect to the AOA.

The gust excitation is applied to the CFD system, and the system is sampled at time intervals corresponding to the CFD time step Δt. The sampling rate is therefore $f_s = 1/\Delta t$, from which signals of

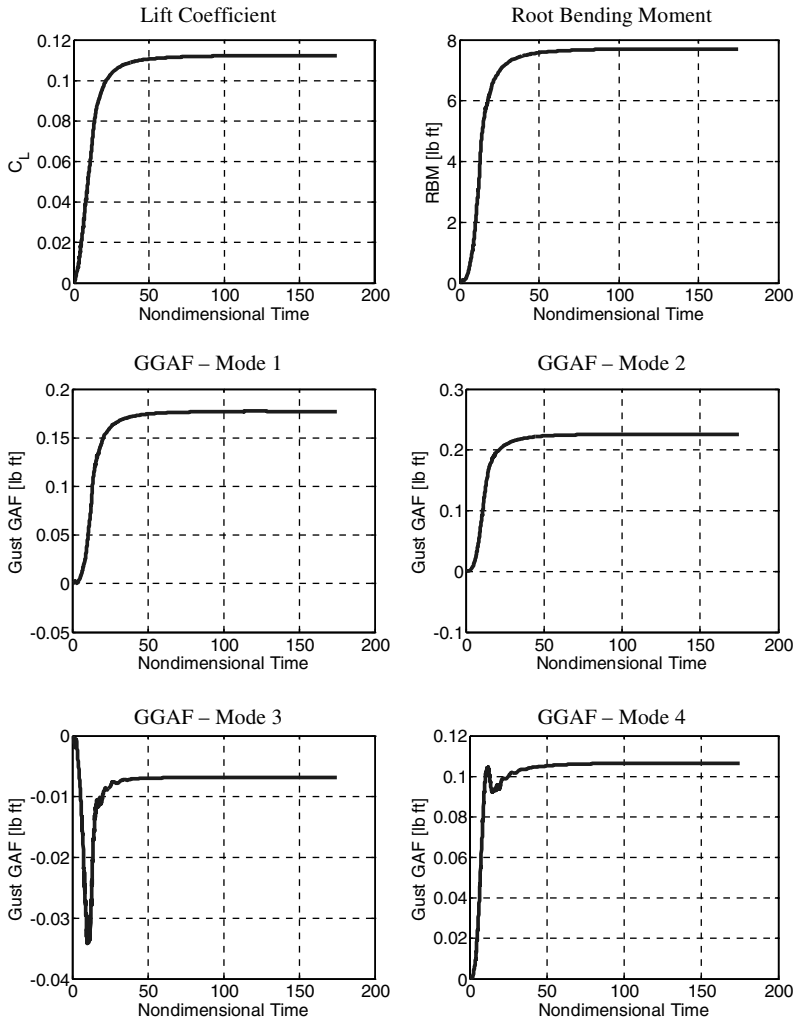

Fig. 4 Responses to sharp-edged gust excitation; 2-deg AOA, Mach 0.2.

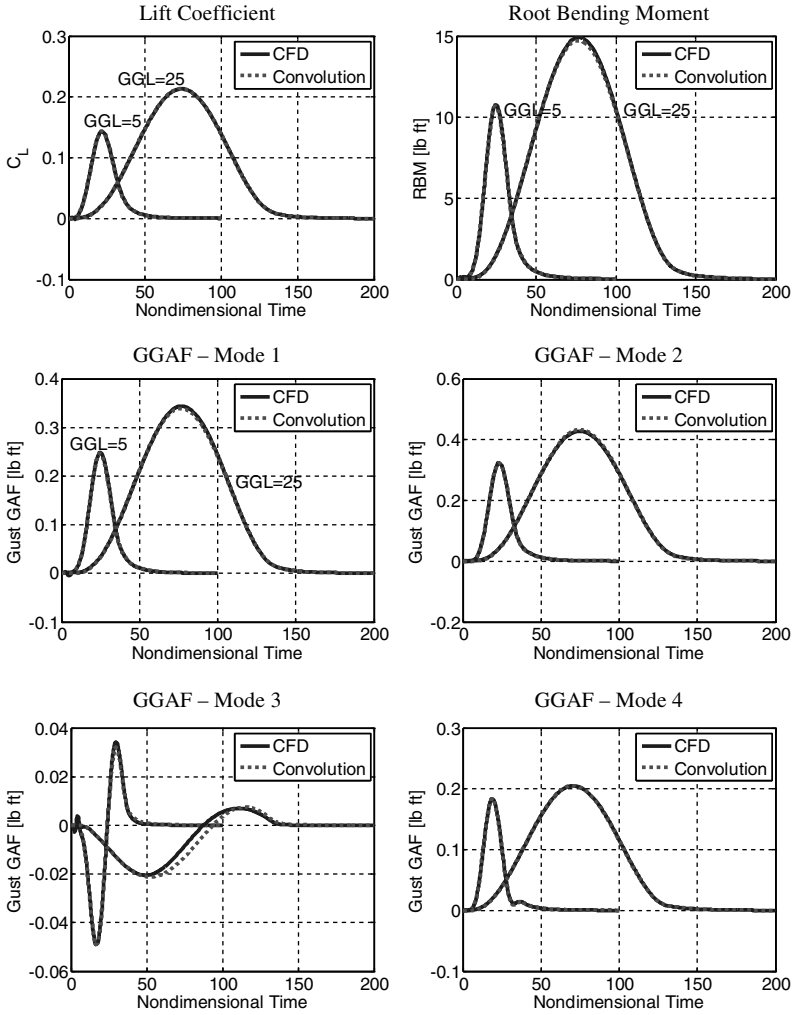

Fig. 5 Responses to one-minus-cosine gust excitations, from CFD simulation and from convolution; 4-deg AOA, Mach 0.2.

frequencies of up to half the sampling rate, denoted by f_{Nyq}, can be reconstructed (based on the Nyquist theorem (see [13], Chapter 13.7, pages 444–445). Because typical CFD time steps are very small, the maximum frequency that can be identified is high and far exceeds the typical frequency range of interest of the aeroelastic problem. The frequency resolution of N, given by f_{Nyq}/N, should be adequate for the representation of the lowest frequencies of interest for the aeroelastic problem. Therefore, the sampling interval and the length of the sampled signal (the number of samples) need to be adjusted to fit the desired frequency range and resolution.

In the current application, the CFD time step was set to $\Delta t = 0.05$ nondimensional seconds (nd-s), based on stability limits of the CFD scheme. This is the largest possible time step for the numerical scheme and the specific test case. From this sampling interval, nondimensional frequencies of up to $f_{\text{Nyq}} = 10$ cycle/nd-s can be reconstructed. A nondimensional frequency of 10 cycle/nd-s corresponds to a dimensional frequency of about 6000 Hz (computed by $f_{\text{nd}} = f \times L_{\text{ref}}/a_{\text{inf}}$ using the reference sea-level speed of sound $a_{\text{inf}} = 1116.4$ ft/s and a reference length of $L_{\text{ref}} = 1.83$ ft). For the AGARD 445.6 wing, the frequency range of interest is bounded by the fourth and highest structural mode at $f = 91.5$ Hz. Thus, it is clear that this sampling rate is sufficiently small, and it can be assumed that all of the frequencies of interest are well represented in the data. A low-pass digital Butterworth filter was applied to the input signal, with a cutoff frequency of $0.02 f_{\text{Nyq}}$, to filter out frequencies above $\sim$120 Hz. The CFD response was recorded over $N = 10,000$ time steps, providing a frequency resolution of 1 E^{-3} cycle/nd-s, or 0.6 Hz. One of the hurdles in system identification is the amount of data required for successful identification. If generating that data requires extremely large computational resources, then the feasibility of the whole approach may be in doubt. Running the CFD code for 10,000 makes a relatively large run, depending on grid dimensions. However, it will be shown in the numerical example that much shorter data sets yield accurate models.

III. Numerical Application

The proposed methodology of this study is demonstrated with the AGARD 445.6 wing [15]. The AGARD 445.6 wing was tested for flutter characteristics in the Transonic Dynamic Tunnel at NASA Langley Research Center and was used as a test case in many studies of transonic aerodynamics [9,16,17]. The current study is not concerned with transonic applications; however, the AGARD 445.6 wing is a useful model because of its known flow and structural elastic properties.

The flow is analyzed using the EZNSS code [8]. EZNSS is a time-accurate implicit finite difference code, based on the Beam and Warming algorithm, which is capable of analyzing the static and dynamic flowfields over a maneuvering elastic vehicle [18]. The problem setup is described in detail in [17]. The CFD mesh is one of typical size for the problem at hand (wing only) and the CFD method (Euler). Initial analyses provided the steady-state inviscid flowfield at Mach numbers 0.2 and 0.8, at zero AOA. The structural modal model of the wing consists of four elastic modes that can be characterized as first bending, first torsion, second bending, and second torsion [15,17].

An EZNSS time-stepping analysis provided the time histories of the lift coefficient, RBM, and four-mode GGAF that developed in response to several types of traveling gust excitations: a sharp-edged gust, a FWGN profile gust, one-minus-cosine gusts, and sinusoidal

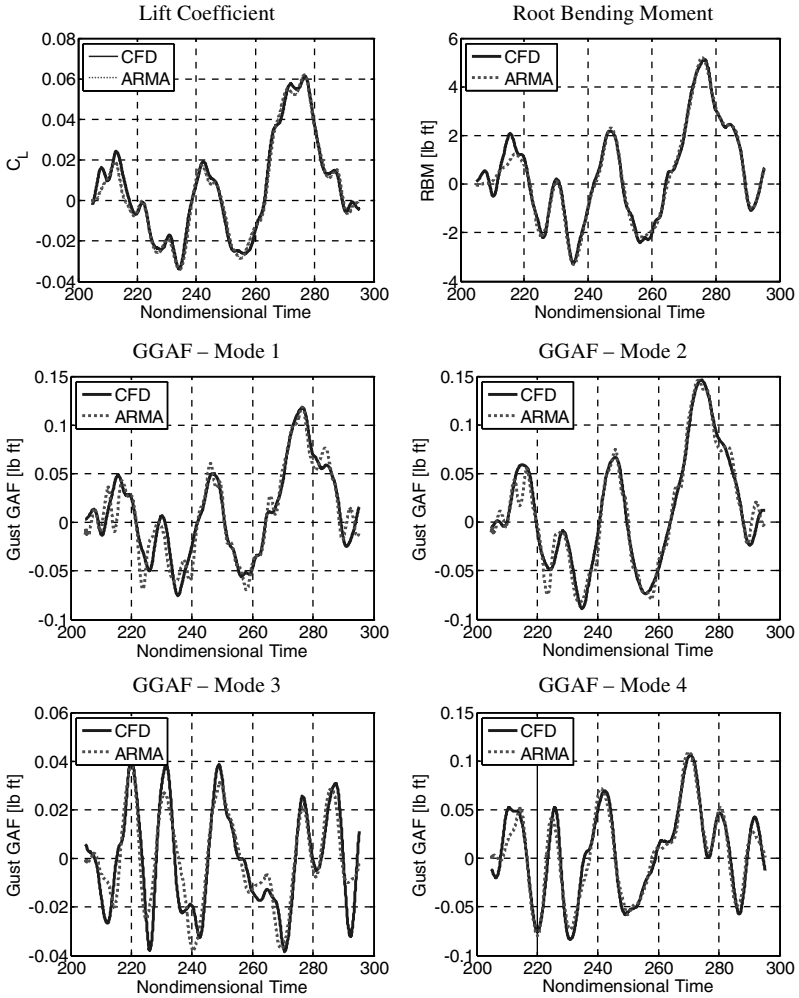

Fig. 6 Responses to filtered white Gaussian noise gust excitation, from CFD simulations and from an 8,8 ARMA model; Mach 0.2.

gusts of various frequencies. The first two served as the identification data sets, from which various gust models were identified. The latter two served for validation of the model results. The one-minus-cosine gust excitation at t at a location x is defined as

$$w_g(t) = \begin{cases} \frac{1}{2}\bar{w}_g\left(1 - \cos\frac{2\pi(t-x/V)}{\mathrm{GGL}c}\right) & \frac{x}{V} < t < \frac{x}{V} + \frac{\mathrm{GGL}c}{V} \\ 0 & \text{otherwise} \end{cases} \tag{25}$$

where GGL is the gust gradient length, in chords, defined in Fig. 3. Figure 3 presents the two one-minus-cosine excitations, with GGL of 5 and 25 chords, that were used in this study.

Figure 4 presents responses to a sharp-edged gust of a 2-deg AOA. These responses were used in a convolution scheme, according to Eq. (3), to compute the responses to the one-minus-cosine gusts of Fig. 3. Figure 5 presents the convolved and direct CFD responses. It is shown that the convolution, using the sharp-edged gust response, predicts the one-minus-cosine responses very accurately. The benefit of the convolution approach is that it only requires one CFD simulation, the sharp-edged gust response, and then responses to any gust excitation can be computed via convolution. Figure 4 shows that the sharp-edged gust response was run over approximately 100 nd-s, which corresponds to 2000 iterations at a time step of 0.05, before it reached its steady-state value. The one-minus-cosine analyses were carried out over about 100 and 200 nd-s for the 5 and 25 GGL, respectively, before reaching steady state, thus amounting to 2000 and 4000 CFD iterations. The time-saving using the convolution approach is evident when many discrete-gust responses, or responses to long excitations, are sought.

A FWGN gust excitation signal, with maximum AOA amplitude of 5 deg, was used for generating identification data for the ARMA and SS models. Part of the training data were used for model identification, whereas the rest of the training data were used for model validation. ARMA and SS models of various sizes were identified, with an emphasis on matching responses at frequencies that range from close to zero to half the Nyquist frequency. Figure 6 presents response time histories of responses to the FWGN validation signal, comparing the simulated ARMA outputs to measured CFD responses. The ARMA model size is $na = 8$ and $nb = 8$. The identification was based on 4096 data points, whereas the rest of the FWGN response data served for model validation and are presented in Fig. 6. It is shown that the ARMA models capture the CFD responses fairly accurately. The response of mode 3 GGAF is somewhat less accurate. However, it is noted that its amplitude is an order of magnitude smaller than those of the other GGAFs, and so this mode is not a large contributor to the loads due to gust excitation.

The models were also examined for their ability to reproduce responses to various gust excitations, namely, one-minus-cosine gusts of two gradient lengths and harmonic sinusoidal gusts of various frequencies. Figures 7 and 8 present one-minus-cosine responses computed with an 8,8 ARMA model and with a four-state SS model, respectively. The models capture all responses well, except for the third-mode GGAF. It is noted that the models of Figs. 7 and 8 were identified based on short data sets (4096 iterations). This makes the proposed method very efficient, especially for large applications, because it does not require a myriad of CFD iterations for successful model identification.

The ARMA and SS models were also tested on their ability to reproduce the system's frequency response. Validation was achieved

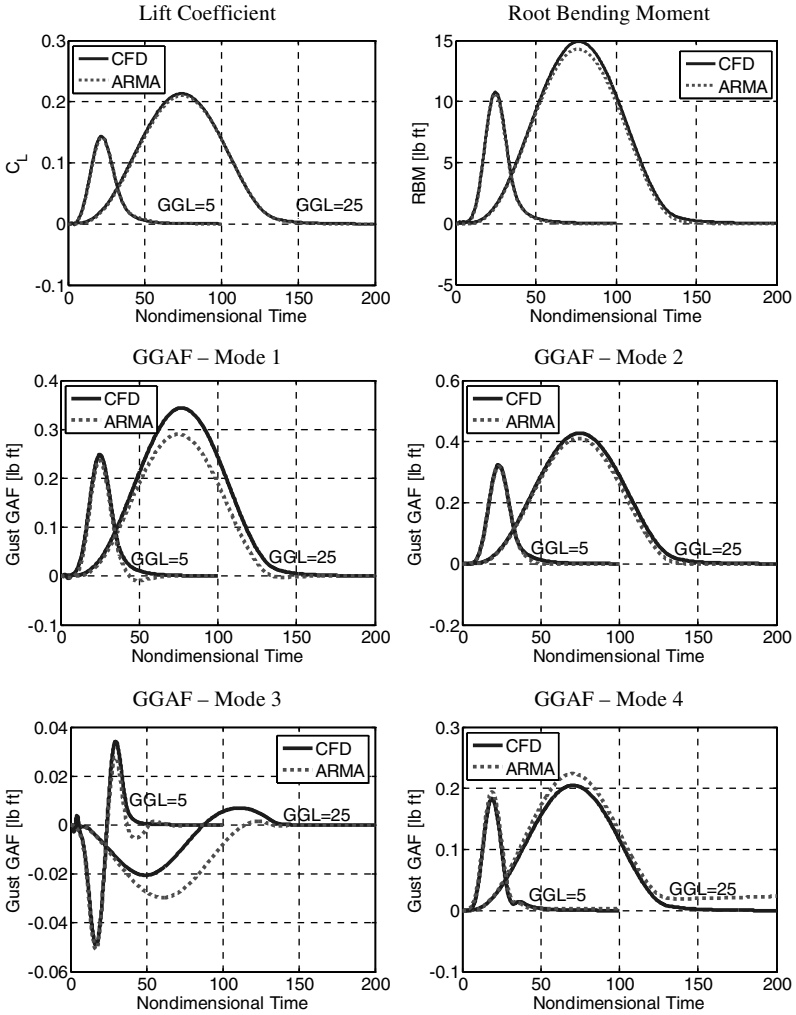

Fig. 7 Responses to one-minus-cosine gust excitations, from CFD simulations and from an 8,8 ARMA model; 4-deg AOA, Mach 0.2.

by frequency sweep: CFD responses were computed to sinusoidal excitations of various frequencies. The CFD analysis was performed over three cycles (or more, for the high frequencies), after which the response reached its steady state, and its real and imaginary parts were computed from the last cycle. Figure 9 presents frequency response of the lift coefficient, from ARMA models of sizes 4,4; 8,8; 10,10; and 20,20 that were identified based on 1024 and 4096 data points (left and right plots, respectively). The validation data, real and imaginary parts of the response from CFD frequency sweep, are presented as the stars in Fig. 9. It is shown that, based on 4096 data points, all model sizes yielded models of good accuracy and that increasing the model size increases its accuracy. It is noted that all the model sizes that were tested are small and very computationally efficient compared with the comprehensive CFD analysis.

CFD gust analysis was repeated at Mach 0.8. At this transonic Mach number, the traveling gust induces a shock wave, its strength depending on the gust velocity magnitude, and the flow characteristics are slightly nonlinear. Linear ARMA models were identified from a ∼9000-iteration CFD response to a FWGN gust excitation of 5-deg AOA and were used to compute responses to one-minus-cosine gust excitations of 2- and 4-deg AOA. These responses were also computed by convolution, using a sharp-edged gust response of 2-deg AOA. Figure 10 presents a comparison of the lift coefficient and RBM responses from these two models with a response computed directly from a CFD simulation. The comparison of Fig. 10 shows that the convolution model captures the response pretty accurately, whereas the ARMA model is somewhat less accurate. The ARMA model accuracy did not improve when a larger model size was used. The issue of reduced-order modeling of gust responses at transonic flows needs to be further explored for flowfields in which nonlinearity is more accented. Currently, it is the full CFD simulation that offers an analysis method that fully captures the nonlinear flow phenomena, whereas convolution offers a very efficient, and relatively accurate, alternative.

A. Aerodynamic Response to Continuous Atmospheric Gust

Federal Aviation Regulations require evaluation of design gust loads by power-spectral methods, for which the gust velocity is modeled by its power-spectral density (PSD) property [19]. Such analysis requires knowledge of the frequency response of the rigid and flexible aircraft and, thus, knowledge of the aerodynamic frequency response, relating the GGAF to the gust input, as a function of frequency. The latter can be extracted straightforwardly from the CFD time histories of the FWGN response by Fourier or spectral analysis or it can be extracted from the time-domain SS or ARMA models (as presented in Fig. 9).

Figure 11 presents the GGAF complex frequency response as real and imaginary parts. Each plot corresponds to a generalized force of one elastic mode. The frequency response was calculated by taking the estimated cross spectral density of the input and output signals $P_{w_g GF_G}(k)$ divided by the PSD of the input signal $P_{w_g w_g}(k)$, according to

$$\boldsymbol{GF}_G(k) = \frac{P_{w_g GF_G}(k)}{P_{w_g w_g}(k)} \tag{26}$$

where $k = \omega c/M$. The frequency-domain GGAF are the so-called gust columns of the frequency-domain gust-analysis formulation [3]. The starts in Fig. 11 are the exact values from direct CFD frequency

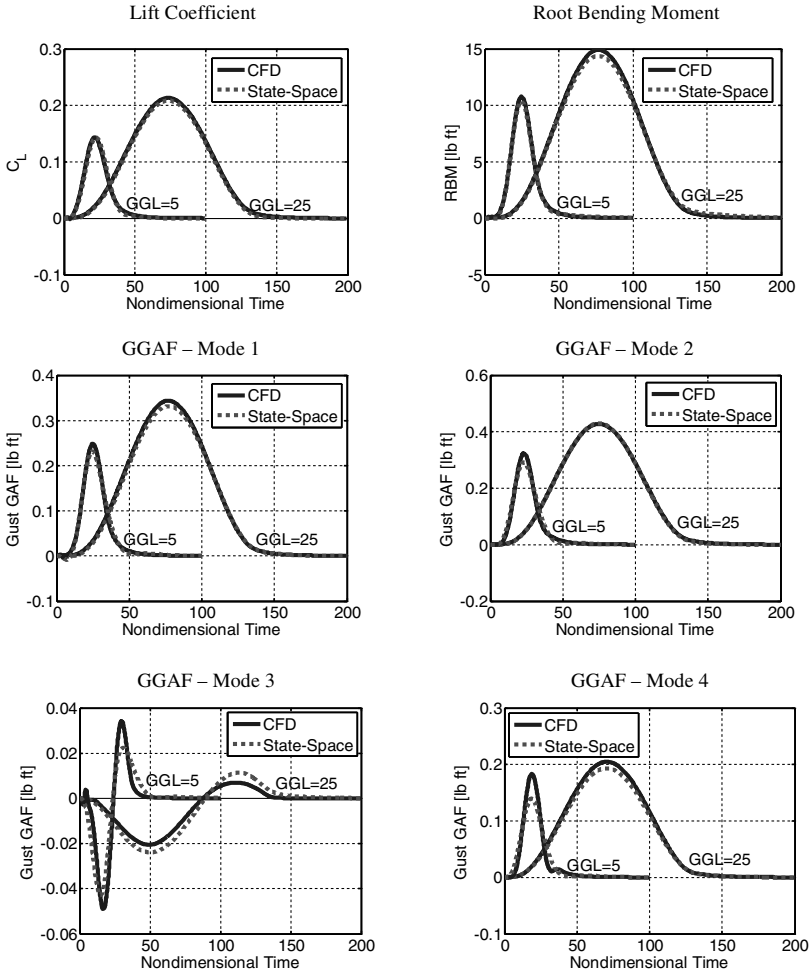

Fig. 8 Responses to one-minus-cosine gust excitations, from CFD simulations and from SS model; 4-deg AOA, Mach 0.2.

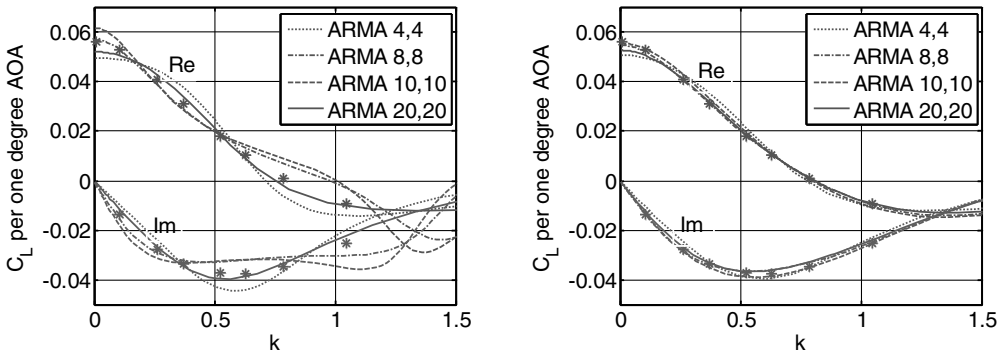

Fig. 9 Frequency response of ARMA models of different size, identified based on training data of a) 1024 points and b) 4096 points; Mach 0.2.

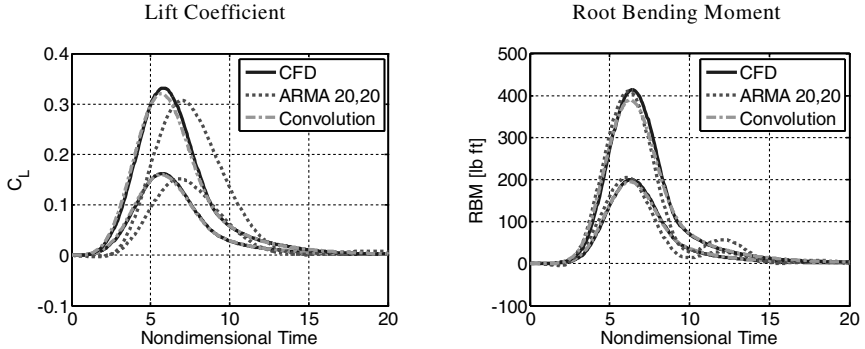

Fig. 10 Responses to one-minus-cosine gust excitations, from CFD simulations, convolution, and a 20,20 ARMA model; 2- and 4-deg AOA, Mach 0.8.

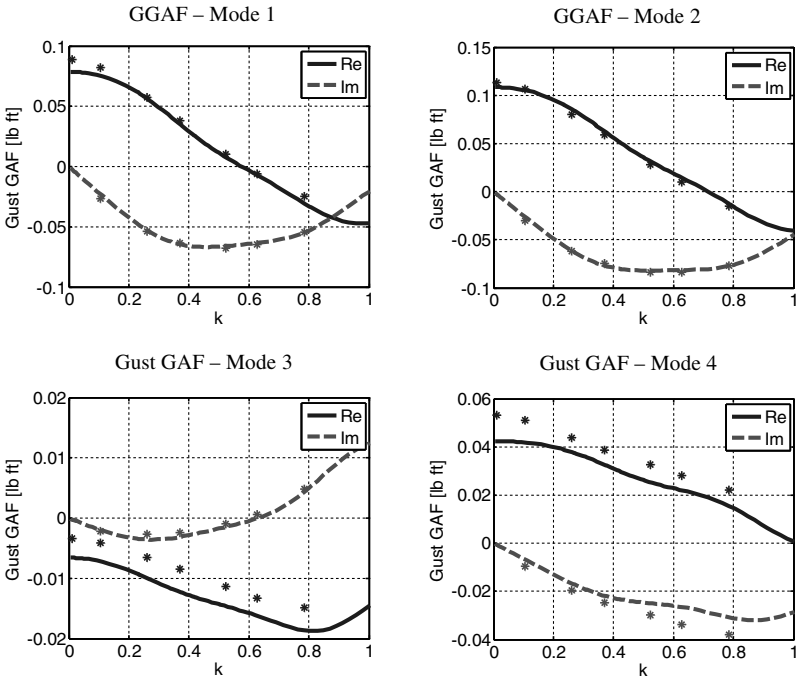

Fig. 11 GGAF frequency response as real and imaginary parts; Mach 0.2.

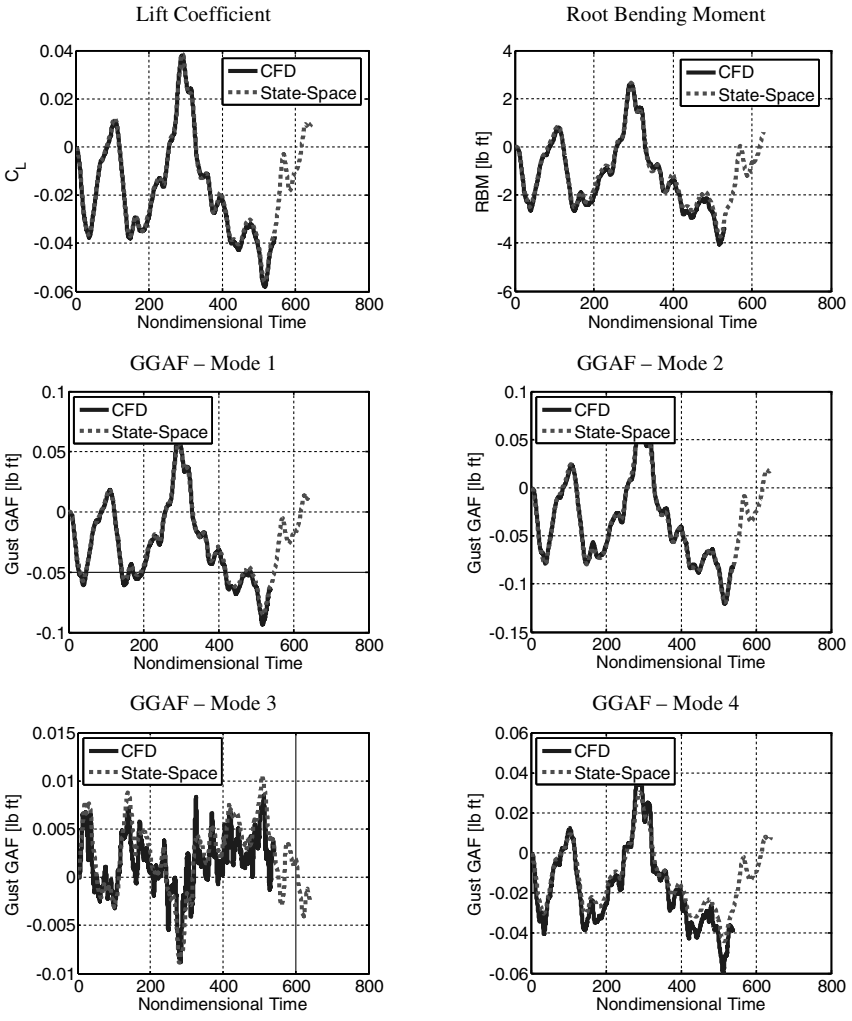

Fig. 12 Responses to Dryden gust input, from CFD simulations and from SS model; 5-deg AOA, Mach 0.2.

sweep. It can be shown that the gust columns are computed accurately for the first two modes and less accurately for modes three and four.

Continuous gust analysis relies on one of two statistical atmospheric gust models, namely, the von Kármán and Dryden models. The Dryden gust model describes the wind gust velocity in terms of its PSD, based on atmospheric measurements. The Dryden PSD for a vertical gust is [20]

$$P_{\text{Dryden}}(\omega) = \sigma_w^2 \frac{L}{V\pi} \frac{1 + 3(L/V)^2\omega^2}{[1 + (L/V)^2\omega^2]^2} \tag{27}$$

where σ_w is the root mean square gust magnitude, taken here as 1, and L is the scale of turbulence, taken here as 2500 ft, according to the FAR. A time-domain Dryden gust input signal can be generated by passing a random signal through a Dryden shaping filter, which is represented by the following transfer function:

$$\boldsymbol{H}_{\text{Dryden}}(S) = \sigma_w \sqrt{\frac{L}{V\pi}} \frac{[\sqrt{3}(L/V)S + 1]}{[(L/V)^2S^2 + 2(L/V)S + 1]} \tag{28}$$

The aerodynamic response to the Dryden gust input can now be computed either via CFD simulation or from the ARMA or SS models that were previously identified and used for discrete-gust responses, as shown in Fig. 12. It is shown that the SS model captures the CFD response very accurately. The CFD response of Fig. 12 was carried out in over 10,000 iterations. However, it is noted that in order to accurately capture the low frequencies, many more iterations are required. For example, as computed previously, two iterations are required to simulate one cycle at 0.37 Hz. Such a simulation would amount to very long computational time compared with the simulation using the already-available SS model, which is performed in seconds.

Finally, the SS model can be used to rapidly compute the system's spectral properties, for example, the RBM PSD in response to Dryden gust excitation. P_{RBM}, the RBM PSD, is computed as

$$P_{\text{RBM}} = |\boldsymbol{H}_{\text{RBM}}|^2 P_{\text{Dryden}}$$

where $\boldsymbol{H}_{\text{RBM}}$ is the frequency response of RBM to gust excitation, and $|\boldsymbol{H}_{\text{RBM}}|$ is the RBM response gain presented in upper right plot in Fig. 9. It is noted that the RBM model, or the model of any other desired section load, is identified directly from the CFD training data.

IV. Conclusions

This paper presented a method for reduced-order modeling of the unsteady aerodynamic forces that develop on a wing in response to traveling gust excitation. Four types of ROMs were identified: a convolution model, ARMA and state-space models (both parametric, time-domain models), and a frequency-response model. All models were based on training data computed in CFD simulations and were reviewed based on their ability to reproduce responses to various gust excitations simulated by direct CFD analyses. In most cases, these models capture the CFD direct response very accurately. The ROMs studied in this research were for the lift coefficient, root-bending moment, and generalized gust forces due to gust excitation. In general, models can be identified for any aerodynamic coefficient, section load, or even local response, such as a panel pressure coefficient. The merit of these models is that they are compact and computationally efficient. They simulate the desired gust responses instantly, compared with the lengthy full CFD simulations. The state-space model can be directly augmented to the aeroelastic system in state-space formulation for rapid aeroelastic response analysis.

References

[1] Anon., "Gust and Turbulence Loads," *Code of Federal Regulations*, Aeronautics and Space, Part 25.341, National Archives and Records Administration, Office of the Federal Register, Jan. 2003.

[2] Anon., "ZAERO Theoretical Manual," Ver. 7.0, Zona Technologies, Scottsdale, AZ, Nov. 2003.

[3] Karpel, M., Moulin, B., and Chen, P. C., "Dynamic Response of Aeroservoelastic Systems to Gust Excitation," *Journal of Aircraft*, Vol. 42, No. 5, Sept.–Oct. 2005, pp. 1264–1272.

[4] Karpel, M., Moulin, B., Anguita, L., Maderuelo, C., and Climent, H., "Aeroservoelastic Gust Response Analysis for the Design of Transport Aircrafts," AIAA Paper 2004-1592, 2004.

[5] Gennaretti, M., and Mastroddi, F., "Study of Reduced-Order Models for Gust-Response Analysis of Flexible Wings," *Journal of Aircraft*, Vol. 41, No. 2, Mar.–Apr. 2004, pp. 304–313.

[6] Tang, D., Kholodar, D., Jer-Nan, J., and Dowell, E. H., "System Identification and Proper Orthogonal Decomposition Method Applied to Unsteady Aerodynamics," *AIAA Journal*, Vol. 39, No. 8, Aug. 2001, pp. 1569–1576.

[7] Zaide, A., and Raveh, D., "Numerical Simulation and Reduced-Order Modeling of Airfoil Gust Response," *AIAA Journal*, Vol. 44, No. 8, Aug. 2006, pp. 1826–1834.

[8] Levy, Y., "Numerical Simulation of Dynamically Deforming Aircraft Configurations Using Overset Grids," *Journal of Aircraft*, Vol. 38, No. 2, 2001, pp. 349–354.

[9] Raveh, D. E., "Identification of Computational-Fluid-Dynamics Based Unsteady Aerodynamic Models for Aeroelastic Analysis," *Journal of Aircraft*, Vol. 41, No. 3, May–June 2004, pp. 620–632.

[10] Parameswaran, V., and Baeder, J. D., "Indicial Aerodynamics in Compressible Flow:Direct Computational Fluid Dynamics Calculations," *Journal of Aircraft*, Vol. 34, No. 1, Jan.–Feb. 1997, pp. 131–133.

[11] Singh, R., and Baeder, J. D., "Direct Calculation of Three-Dimensional Indicial Lift Response Using Computational Fluid Dynamics," *Journal of Aircraft*, Vol. 34, No. 4, July–Aug. 1997, pp. 465–471.

[12] Singh, R., and Baeder, J. D., "Generalized Moving Gust Response Using CFD with Application to Airfoil-Vortex Interaction," AIAA Paper 97-2208, 1997.

[13] Ljung, L., *System Identification: Theory for the User*, 2nd ed., Prentice–Hall, Upper Saddle River, NJ, 1999.

[14] Franklin, G. F., and Powell, D., *Digital Control of Dynamic Systems*, 1st ed., Addison–Wesley, Philippines, 1980, Chap. 6, pp. 131–139.

[15] Yates, E. C., Jr., "AGARD Standard Aeroelastic Configurations for Dynamic Response, Candidate Configuration 1: Wing 445.6," NASA TM-100492, 1987.

[16] Lee-Rausch, E. M., and Batina, J. T., "Wing Flutter Boundary Prediction Using Unsteady Euler Aerodynamic Method," *Journal of Aircraft*, Vol. 32, No. 2, 1995, pp. 416–422.

[17] Raveh, D., Levy, Y., and Karpel, M., "Efficient Aeroelastic Analysis Using Computational Unsteady Aerodynamics," *Journal of Aircraft*, Vol. 38, No. 3, 2001, pp. 547–556.

[18] Raveh, D., Levy, Y., and Karpel, M., "Structural Optimization Using Computational Aerodynamics," *AIAA Journal*, Vol. 38, No. 10, 2000, pp. 1974–1982.

[19] Anon., "Continuous Gust Design Criteria," *Code of Federal Regulations*, Aeronautics and Space, Appendix G to Part 25, National Archives and Records Administration, Office of the Federal Register, Jan. 2003.

[20] Hoblit, F. M., *Gust Loads on Aircraft: Concepts and Application*, AIAA Education Series, AIAA, Washington D.C., 1988, Chap. 4.5.